

S2D: Sparse to Dense Lifting for 3D Reconstruction with Minimal Inputs

Yuzhou Ji¹, Qijian Tian¹, He Zhu¹, Xiaoqi Jiang⁴, Guangzhi Cao⁴, Lizhuang Ma¹, Yuan Xie², Xin Tan^{2,3*}

¹Shanghai Jiao Tong University ²East China Normal University

³Shanghai Artificial Intelligence Laboratory ⁴Chery Automobile

jyuzhou@sjtu.edu.cn xtan@cs.ecnu.edu.cn



Figure 1. **We demonstrate S2D in different situations.** S2D supports reconstruction with inputs of different density. The 3DGS scene reconstructed through S2D is free of severe artifacts that occur in traditional reconstruction under sparse inputs. S2D also outperforms state-of-the-art scene enhancer (DIFIX) and direct video generation conditioned on camera poses (SEVA).

Abstract

Explicit 3D representations have already become an essential medium for 3D simulation and understanding. However, the most commonly used point cloud and 3D Gaussian Splatting (3DGS) each suffer from non-photorealistic rendering and significant degradation under sparse inputs. In this paper, we introduce Sparse to Dense lifting (S2D), a novel pipeline that bridges the two representations and achieves high-quality 3DGS reconstruction with minimal inputs. Specifically, the S2D lifting is two-fold. We first present an efficient one-step diffusion model that lifts sparse point cloud for high-fidelity image artifact fixing. Meanwhile, to reconstruct 3D consistent scenes, we also design a corresponding reconstruction strategy with random sample drop and weighted gradient for robust model fitting from sparse input views to dense novel views. Extensive ex-

periments show that S2D achieves the best consistency in generating novel view guidance and first-tier sparse view reconstruction quality under different input sparsity. By reconstructing stable scenes with the least possible captures among existing methods, S2D enables minimal input requirements for 3DGS applications. Project page at <https://george-attano.github.io/S2D>.

1. Introduction

While pure vision language models still show certain limitation in spatial understanding due to 2D inputs, 3D Gaussian Splatting (3DGS) [19] has long been playing an important role in autonomous driving and embodied AI simulation. However, the rendering quality of 3DGS degrades significantly when the viewing angle deviates from input poses, which requires a large amount of input to maintain low view interpolation distance. In real-life circumstances, it is unre-

*Corresponding author.

alistic to always ensure dense input, not to even mention the corresponding computational cost. Therefore, the practical application based on 3DGS has been severely hindered.

To get rid of the long-lasting constraint of input requirements hovering upon 3DGS, the ultimate goal is to achieve photorealistic reconstruction with minimal inputs. With this aim, we first define the most demanding sparse input setting to be acquiring the same viewing range as in point cloud reconstruction. For example, with only one input image, the reconstructed scene can be viewed within 30° spiral angles, and can stably provide more than 180° view range with less than 10 input images. In such a setting, traditional reconstruction methods are corrupted as shown in Figure 1.

To solve this problem, some try to build a feed-forward models [6, 7, 17, 40, 42, 44, 51, 62, 63, 73] that directly predicts gaussian attributes, but still creates much artifacts in this scenario (as in Figure 4). While object-centric methods [41, 66, 81] can not be applied to general reconstruction, others try to directly generate novel views through diffusion models conditioned on camera extrinsics or sparse points [45, 55, 56, 71, 79], but fail to maintain 3D consistency and generation fidelity, which also require high time consumption. Instead, the recent DIFIX [58] builds a generative fixer that can remove novel view artifacts, which supports scene reconstruction with relatively sparser inputs. However, DIFIX is built upon small view deviation and only operates on mild artifacts. Meanwhile, DIFIX overlooks the gap between novel guidance and real input and directly conduct reconstruction, causing severe 3D inconsistency. In our settings, DIFIX completely fails in sparse inputs, leaving this challenge far from solved.

While 3D consistency and guidance have become a common obstacle in the methods mentioned above, the latest vision foundation models (VFM) [18, 48, 54] have revolutionized 3D prediction, which can conduct dense point cloud reconstruction instantly. Although point cloud requires few input images and is naturally view independent, its rendering is far from photorealistic, with noticeable noise due to aliasing and cumulative error, constraining its application in image-level guidance.

To address the aforementioned challenges, in this paper, we present Sparse to Dense lifting (S2D), a flexible framework that provides high-quality 3DGS reconstruction with extremely sparse inputs. Specifically, we first contribute a strong yet efficient one-step diffusion model that lifts the sparse point cloud for high-fidelity image artifact fixing. With pixel-level details provided by the input view and structural guidance in point cloud rendering, our fixing model is able to handle extreme artifacts while still providing excellent consistency across views. For better fitting the 3DGS optimization under sparse inputs and dense fixed guidance, we also propose a corresponding reconstruction strategy with random sample drop and weighted gradient.

Extensive experiments show that S2D achieves the best consistency in generating novel view guidance and first-tier sparse view reconstruction quality among various methods.

Notably, S2D is not fixed in the input number and supports any input density, which is suitable for general reconstruction enhancement.

In summary, this work has the following contributions:

- We propose S2D, a flexible framework for baseline 3DGS methods to conduct sparse-view reconstruction, supporting view extrapolation and larger view interpolation.
- We present a strong yet efficient artifact-fixing model that can take both input view and novel view point cloud rendering as guidance, achieving first-tier quality in removing image artifacts.
- We design a reconstruction strategy for better model fitting and 3D consistency under sparse input and dense novel guidance.

2. Related Work

2.1. Gaussian Splatting

After first introduction, 3D Gaussian Splatting (3DGS) [19] has expanded upon largely with further innovations [26, 31, 39, 60]. Many contributions [7, 24, 61, 78] underscore the ongoing enhancements and versatility of 3DGS in handling increasingly complex rendering tasks. Despite the advantages of 3D Gaussian Splatting in rendering speed and quality, the results degrade significantly with the reduction of input training views, limiting the applicable scenarios.

To this end, feed-forward 3DGS models [6, 7, 17, 40, 42, 44, 51, 62, 63, 70, 73] have emerged to handle reconstruction with fewer inputs. In particular, pixelSplat [6] and Splatter Image [40] predict Gaussian attributes from image features, while MVSpLat [7] encodes the feature matching information with cost volumes. DepthspLat [62] further integrates monocular features from pre-trained monocular depth models and achieves more robust depth prediction and 3D Gaussian reconstruction.

Although these methods improve quality and efficiency in sparse-view reconstruction, the lack of explicit 3D supervision limits generalization of pre-trained models and is still unable to handle extreme inputs.

2.2. Universal 3D reconstruction

Feed-forward models has advanced even more significantly in point cloud reconstruction while predicting multiple 3D attributes. The early DUST3R [50] and MAST3R [20] predict a coupled scene representation but require further post-processing. The following works expand them towards more pipelines [11, 12, 27, 30] and support extra input views [3, 47, 49], but still provide limited quality compared to traditional optimization.

Recently, multi-view models such as VGGT [48] have

made excellent progress in 3D prediction, with many valuable efforts in more accurate localization [10, 43] and longer sequences [9, 68]. Notably, π^3 [54] employs a fully permutation-equivariant architecture and achieves higher robustness. Later, MapAnything [18] further enables a broad range of 3D vision tasks in a single feed-forward pass, pushing such models to real-world applications. While these methods do not directly support photorealistic view synthesis, we utilize them as strong structural consistent guidance for image level lifting.

2.3. Reconstruction with diffusion prior

Advancements in image and video diffusion models [2, 32, 34, 52, 69] have achieved highly controlled generation, making it possible to leverage diffusion prior as photorealistic guidance for scene reconstruction. In autonomous driving simulation, it has already been a popular solution to distill customized video generation to dynamic scene reconstruction [28, 53, 65, 75–77]. Concerning common static scenarios, diffusion-based novel view synthesis methods have also evolved from object-level to scene-level [5, 13, 14, 23, 36, 45, 46, 55–57, 59, 71, 79], but their generalization ability, time consumption, and 3D consistency are still far from practical applications.

The recent DIFIX3D+ [58] trains an image diffusion model that takes in surround view reference to restore novel view artifacts as extra guidance, achieving efficient reconstruction with extrapolated views. However, Difix significantly degrades when faced with extreme artifacts under large view deviation, hindering its further applications.

In contrast, S2D gets rid of these limitations and provides efficient and consistent sparse-view reconstruction with structurally guided artifact fixing and lifting.

3. Method

3.1. Overview

The general pipeline of S2D is shown in Figure 2 Left. Given any number of input views and novel cameras, we firstly generate the point cloud using VFM [18, 48, 54] and render views on novel cameras. Then we initialize the 3DGS scene on input views until sample iteration it_s . At it_s , a single round of rendering on all novel cameras is conducted. The resulting novel view images containing artifacts are then sent through our artifact fixer (detailed structure in Figure 2 Right) along with a nearby input view as reference and the corresponding point cloud rendering. After removing artifacts, we continue to optimize the scene with mixed supervision from input views and novel view results until final iteration it_e , where random sample drop and weighted gradient are employed. Finally, we obtain the consistent 3DGS scene with largely expanded view range.

3.2. Initialization

Given any input views, we conduct simple initialization. We sent the original views through VFM (π^3 [54] with default setting in practice) to acquire the sparse point cloud of the scene. A set of novel cameras can be automatically generated (e.g. through interpolation or preset extrapolation offsets) or manually set according to needs. We render views of the point cloud on these views as later guidance.

3.3. Novel view artifact fixer

While the distillation of video diffusion suffers from high consumption [28, 59, 65, 76], methods based on image enhancement also show incompetence in extreme situations [13, 58]. In this work, we build a generative artifact fixer upon one-step diffusion model yet supports strong structural guidance, which provides both high efficiency and quality.

One-step diffusion model. In Latent Diffusion Models (LDM) [34], the data x_t is encoded into a latent representation z_t via the perceptual compression encoder \mathcal{E} , and samples from data distribution $p(z)$ is decoded to image space with a single pass through decoder \mathcal{D} . LDM realizes the neural backbone $\epsilon_\theta(o, t)$ as a time-conditional UNet [35], with the simplified objective as:

$$L_{LDM} = \mathbb{E}_{\mathcal{E}(x), \epsilon \sim \mathcal{N}(0,1), t} \left[\|\epsilon - \epsilon_\theta(z_t, t)\|_2^2 \right]. \quad (1)$$

In pix2pix-turbo [29], the backbone \mathcal{E} , \mathcal{D} and ϵ_θ are fine-tuned at fixed timestep t_d so that image translation can be efficiently conducted through a single denoising step instead of multiple steps.

Dual guidance. The state-of-the-art method Difix [58] uses nearby views as reference for artifact fixing, which mainly provides texture guidance that fixes blurry regions but fails in larger artifacts and corrupted structure.

While point cloud is naturally view independent and structurally consistent, we introduce dual guidance for artifact fixing. For each novel view rendering, it is fixed with both corresponding point cloud rendering and nearby reference. Although accurate point cloud can serve as strong hint for details, noise is currently inevitable due to aliasing and cumulative error, thus we design a mixing module to determine the sample of guidance so that only valuable parts should be considered.

The model architecture of our artifact fixer is shown in Figure 2 Right. Specifically, in the early mixing module, we extract both DINO features and images features of target view and corresponding point cloud guidance. The features go through project layers and combined. After cross attention step, the embeds are lifted to generate a mixed input image. This mixing module is designed to encourage better usage of point cloud guidance (see ablations in Sec 5.1).

The mixed image I^m and reference image I^r are encoded through VAE encoder \mathcal{E} to obtain latent representa-

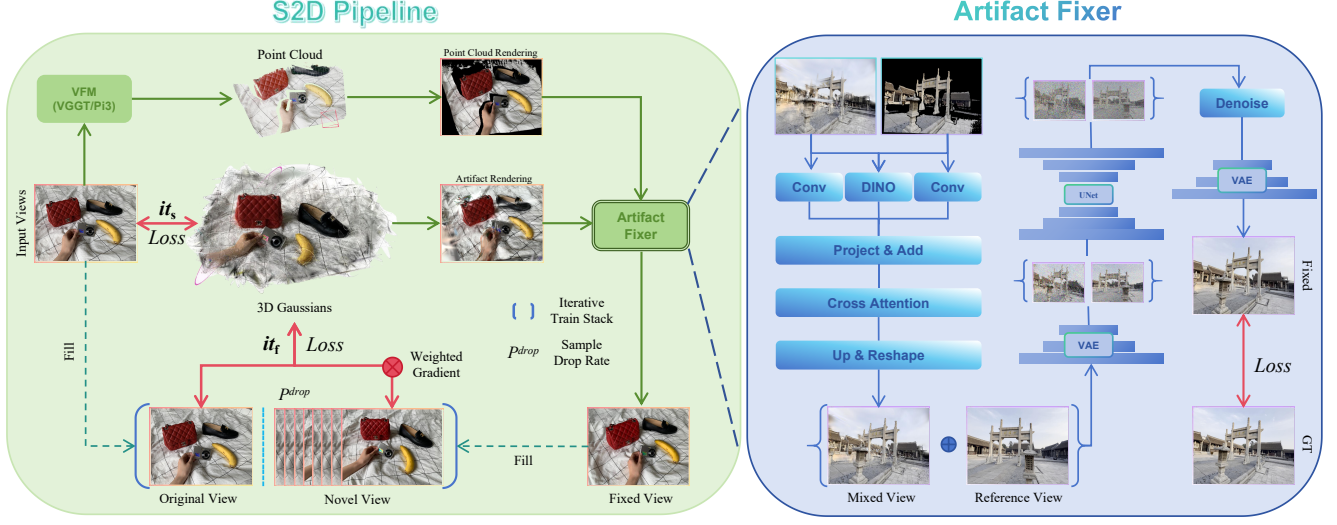


Figure 2. S2D reconstruction pipeline and model architecture of artifact fixer.

tion z :

$$[z^m, z^r] = \mathcal{E}([I^m, I^r]), \quad (2)$$

and the noise sample Z at fixed timestep t_d is predicted by multi-view time-conditional UNet [58]:

$$[Z^m, Z^r] = \epsilon_\theta([z^m, z^r], t_d). \quad (3)$$

We discard Z^r and conduct single step denoise conditioned on z^m :

$$z^d = \frac{\sqrt{\xi_{t-1}} \cdot \eta_t}{\eta_{t-1}} \cdot Z^m + \frac{\sqrt{\xi_t} \cdot \eta_{t-1}}{\eta_t} \cdot z^m + \sigma_t \cdot \epsilon_t, \quad (4)$$

where $t = t_d$, and finally decode z^d to fixed image I^{fix} :

$$I^{fix} = \mathcal{D}(z^d). \quad (5)$$

Train artifact fixer. We first generate paired training data. We train DL3DV-960-10K scenes on 3DGS on 4000 iterations with 25 to 50 sample intervals to obtain novel view images with different levels of artifacts. Apart from this sparse reconstruction method, we also apply random perturbations to both the position and rotation attributes of Gaussians at rendering time to generate more artifacts. The rendering time position $\mathbf{x}'_i \in \mathbb{R}^3$ is generated by:

$$\mathbf{x}'_i = \mathbf{x}_i + \epsilon_i^{\mathbf{x}}, \quad \epsilon_i^{\mathbf{x}} \sim \mathcal{N}(0, \sigma_x^2 \mathbf{I}_3) \quad (6)$$

where $\mathbf{x}_i \in \mathbb{R}^3$ is the original 3D coordinate of the i -th Gaussian, and σ_x controls the magnitude of the positional perturbation ($\sigma_x \in [10^{-4}, 10^{-2}]$). The rendering time rotation is generated by:

$$\mathbf{q}'_i = \mathbf{q}_{\epsilon_i} \otimes \mathbf{q}_i \quad (7)$$

The random rotation quaternion \mathbf{q}_{ϵ_i} is generated from an axis-angle representation:

$$\mathbf{q}_{\epsilon_i} = \left[\cos \frac{\phi_i}{2}, \mathbf{k}_i \sin \frac{\phi_i}{2} \right] \quad (8)$$

where $\mathbf{q}_i \in \mathbb{H}$ is the original unit quaternion, $\mathbf{k}_i \sim \mathcal{U}(\mathbb{S}^2)$ is a random unit vector (rotation axis), $\phi_i \sim \mathcal{U}[-\delta_\phi, \delta_\phi]$ is a random rotation angle ($\delta_\phi \in [5^\circ, 45^\circ]$), \otimes denotes quaternion multiplication (Hamilton product).

We input all views to VFM to align test cameras, but the corresponding point cloud images are only rendered with points reconstructed from the same sample views.

We use pix2pix-turbo [29] as the backbone of our artifact fixer, and initialize UNet weights from SD-Turbo [37] and VAE weights from Difx [58]. We train the mixing module and LoRA [16] adapters applied on VAE and UNet modules. Loss is computed against fixed images and ground truth images. We replace the CLIP [33] loss in the backbone with DINO feature loss (as in cosine similarity) and add Similarity Index Measure (SSIM), and inherit the original GAN loss. So the final loss term is:

$$\mathcal{L} = 0.2\mathcal{L}_{LPIPS} + 0.4\mathcal{L}_2 + 0.25\mathcal{L}_{SSIM} + \mathcal{L}_{GAN} + \mathcal{L}_{DINO}. \quad (9)$$

3.4. Reconstruction with novel guidance

With extremely sparse inputs, it is also a challenge to avoid overfitting on novel views and underfitting on input views. For example, extrapolated views may have regions that are not exist within the original view range, and inconsistency could occur in parts with rich textures, which also causes severe artifacts. Previous methods either overlook this problem or simply use smaller weights on novel views

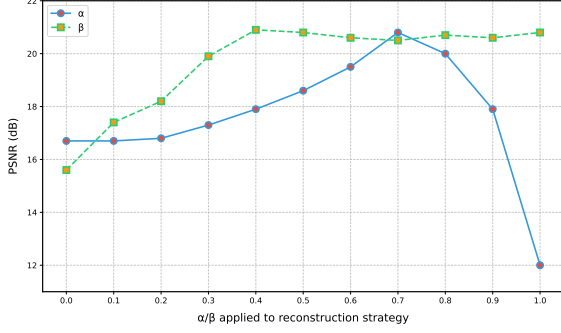


Figure 3. Evaluation on parameter α and β .

[28, 65, 76], which introduces an unavoidable optimization bias and fails to account for the inherent gap between input and novel viewpoints. In this paper, we propose random sample drop and weighted gradients for stable optimization under such circumstances.

Random sample drop. To mitigate quantitative gap between original views and novel views in the supervision set (e.g. a large expansion including 6 input views and 300 novel views), we adopt a probabilistic sampling strategy in training to ensure that original views can provide continuous and sufficient supervision while expanding to novel views. The reconstruction process with is random sample drop depicted in Algorithm 1.

Specifically, given input reference views V_{ref} and novel views V_{novel} , we aim to build a final sample sequence $S_p = [s_1, s_2, \dots, s_N]$ where samples from different view sets are evenly interleaved and satisfy:

$$\frac{|S_{ref}|}{|S_{novel}| + |S_{ref}|} = \alpha. \quad (10)$$

Here S_{ref} and S_{novel} refer to samples from V_{ref} and V_{novel} , and α is the weight to drop novel samples. We test the difference of taking different α values, and the results from a set of DL3DV scenes is shown in Figure 3, where $\alpha = 0$ means complete drop on input views and $\alpha = 1$ means complete drop on novel views. Therefore, in practice, we set α at 0.7.

During training, every drawn sample can be discarded with a dropped probability defined as follows:

$$P^{drop} = \begin{cases} 1 - \min(1, \frac{\alpha}{r_i}), & \text{if } s_i \in V_{ref} \\ 1 - \min(1, \frac{1-\alpha}{1-r_i}), & \text{if } s_i \in V_{novel} \end{cases}, \quad (11)$$

$$r_i = \frac{|\{s_j | j < i, s_j \in S_{ref}\}|}{|\{s_j | j < i\}|}. \quad (12)$$

The sampling strategy generates an interleaved sample sequence and stably controls the proportion of two types of guidance in the training set, providing more stable supervision signals during training.

Algorithm 1: Reconstruction process with random sample drop

Parameters: Iterative view sampling stack S , input reference views V_{ref} , novel views V_{novel} , sample iteration it_s , final iteration it_e , 3DGS representation R , weight α for random sample drop

Output: well-optimized 3DGS representation R

Initialize : $i \leftarrow 0$. // Iteration
 $r \leftarrow 1e - 6$. // For P^{drop} update.

for $i = 1$ to it_s **do**

\perp Optimize R with reference views.

for $i = it_s$ to it_e **do**

if S is empty **then**

$\perp S = \text{shuffle}(S_{ref} + S_{novel})$.

 Get next sample s from S .

 Determine whether to drop s according to

$P^{drop}(s, \alpha, r)$.

 Update r .

if not to drop then

\perp Optimize R with s .

 Update i .

return R

Weighted gradient. In terms of large artifacts that severely corrupt novel views, certain bias between ground truth and novel guidance is inevitable. Previous methods ignore this problem [58, 75] or adopt a general weight [28, 65, 76] on novel views, overfitting to incorrect details. Instead, we design a pixel-level weight $\mathbf{W} \in [0, 1]^{H \times W}$ for each view based on a confidence mask \mathbf{M}^{conf} to reduce the adverse impact of possibly inconsistently fixed regions on Gaussian model training:

$$\mathbf{W}_i(x, y) = \begin{cases} \beta + (1 - \beta)\mathbf{M}_i^{conf}(x, y), & s_i \in V_{novel} \\ 1, & s_i \in V_{ref}, \end{cases} \quad (13)$$

where weight parameter β is also tested as shown in Figure 3. While $\beta = 1$ means no weighted gradient, we set β to 0.4 for better artifact suppression and overall quality. The confidence mask \mathbf{M}^{conf} is calculated by point cloud rendering of a training view v :

$$\mathbf{M}_v^{conf}(x, y) = \mathbb{I}((x, y) \in \mathcal{P}), \quad (14)$$

where \mathcal{P} refers to valid pixels projected by the point cloud, \mathbb{I} refers to indicator function. For a splatted gaussian g_i , the gradient $\nabla_i L$ based on \mathbf{W}_i is calculated as follows:

$$\nabla_i L = \frac{1}{|\mathcal{P}_i|} \sum_{x, y \in \mathcal{P}_i} \mathbf{W}_i(x, y) \frac{\partial L}{\partial G_i(x, y)},$$

where \mathcal{P}_i denotes pixels set g_i splats on, $G_i(x, y)$ denotes the gaussian function value on (x, y) . Due to the constraint



Figure 4. Qualitative results in different situations.

of W_i on pixels, regions containing potential artifacts will contribute less in backpropagation process.

While the artifact fixing is reliable with strong guidance from point cloud, regions without any point cloud but with large artifacts can update the corresponding Gaussian parameters more conservatively with the above strategy. This avoids oscillation or failure of gaussian model by dominating the optimization process with input views and point cloud guidance, providing better 3D consistency.

Ablations of the method can be found in Sec 5.

4. Experiments

We conduct extensive experiments including indoor scenes, outdoor scenes and driving scenes for evaluation, providing both quantitative and qualitative results.

4.1. Implementation Details

Our artifact fixer is trained using the train split of DL3DV-960 [8, 21], including around 2.1M image pairs. The processing for paired data curation (detailed in Sec 3.3) took 850 H200 GPU hours, and the fixing model is trained on 8 H200 GPU for 60 hours with a per-GPU batch size of 4. Evaluation is conducted on a single RTX 4090 GPU for a more general comparison of user side performance. Sample

iteration it_s is set to 3,000 for static scene reconstruction, and 7,000 for driving scene reconstruction. Final iteration it_e is fixed to 30,000 for all scenes. We use 3DGS [19] as reconstruction backbone for S2D and DIFIX, other methods all follow their original settings. For pure generative methods, structural metrics are not applied because they do not support precise camera control on long sequences with all test cameras included in a single run. More implementation details can be found in Appendix.

4.2. Datasets and Metrics

For indoor and outdoor scene reconstruction, we use 3DOVS [22], MIP360 [1] and the test split of DL3DV-960 [8, 21] and RE10K [80]. For driving scene artifact removal and reconstruction, we use Waymo Open Dataset [38].

To evaluate the structural quality of scene reconstruction, we use the peak signal-to-noise ratio (PSNR) and similarity index measure (SSIM). We also report perceptual distance (LPIS) [74] and fréchet inception distance (FID) [15] for perceptual quality, especially in driving scenes with no ground truth provided in extrapolated trajectories.

4.3. Comparison on in-the-wild scenes

We compare the reconstruction quality of our method with baseline 3DGS, feed-forward methods and also generative

| Datasets | 3DOVS @ 1 Image | | | | RE10K @ 2 Images | | | | MIP360 @ 6 Images | | | | DL3DV @ 6 Images | | | |
|-------------------|-----------------|-----------------|--------------------|------------------|------------------|-----------------|--------------------|------------------|-------------------|-----------------|--------------------|------------------|------------------|-----------------|--------------------|------------------|
| | PSNR \uparrow | SSIM \uparrow | LPIPS \downarrow | FID \downarrow | PSNR \uparrow | SSIM \uparrow | LPIPS \downarrow | FID \downarrow | PSNR \uparrow | SSIM \uparrow | LPIPS \downarrow | FID \downarrow | PSNR \uparrow | SSIM \uparrow | LPIPS \downarrow | FID \downarrow |
| 3DGS[19] | 10.12 | 0.30 | 0.69 | 278.9 | 21.14 | 0.61 | 0.36 | 64.3 | 17.14 | 0.48 | 0.41 | 71.9 | 15.26 | 0.51 | 0.46 | 97.7 |
| Mip-Splatting[72] | 11.31 | 0.29 | 0.61 | 249.6 | 21.35 | 0.65 | 0.31 | 63.2 | 16.33 | 0.44 | 0.48 | 91.3 | 18.50 | 0.59 | 0.41 | 86.3 |
| ScaffoldGS[25] | 10.50 | 0.23 | 0.62 | 230.4 | 20.96 | 0.60 | 0.32 | 67.6 | 16.02 | 0.35 | 0.46 | 162.2 | 17.41 | 0.60 | 0.39 | 89.7 |
| NoPoSplat[70] | - | - | - | - | 24.30 | 0.70 | 0.36 | 41.0 | 15.48 | 0.37 | 0.46 | 91.4 | 18.11 | 0.50 | 0.41 | 86.4 |
| AnySplat[17] | 17.91 | 0.48 | 0.42 | 67.0 | 24.32 | 0.69 | 0.35 | 40.6 | 18.12 | 0.60 | 0.44 | 96.4 | 17.39 | 0.59 | 0.43 | 85.3 |
| DepthSplat[62] | - | - | - | - | 25.79 | 0.76 | 0.33 | 38.9 | 19.24 | 0.61 | 0.40 | 84.2 | 19.62 | 0.68 | 0.37 | 81.4 |
| ViewCrafter[71] | - | - | 0.36 | 71.2 | - | - | 0.30 | 39.2 | - | - | - | - | - | - | - | - |
| SEVA[79] | - | - | 0.33 | 67.3 | - | - | 0.29 | 37.4 | - | - | 0.36 | 60.2 | - | - | 0.30 | 52.8 |
| DIFIX[58] | 14.10 | 0.47 | 0.56 | 98.2 | 26.11 | 0.80 | 0.28 | 40.2 | 19.43 | 0.60 | 0.38 | 70.3 | 20.4 | 0.72 | 0.32 | 55.3 |
| S2D (Ours) | 21.41 | 0.77 | 0.27 | 54.0 | 27.62 | 0.86 | 0.24 | 34.7 | 20.97 | 0.70 | 0.35 | 58.1 | 23.2 | 0.81 | 0.26 | 41.2 |

Table 1. Quantitative results in in-the-wild scenes.

methods. For front-facing scenes in 3DOVS, we use only one image as input. For other datasets with larger camera movements, we use six images as input.

Quantitative results. The quantitative results are reported in Table 1. Under such extreme inputs, both traditional methods and state-of-the-art feed-forward methods show significant degradation. Generative methods shows good ability in perceptual quality, but cannot consistently support long sequence with precise camera control, which is not suitable for explicit 3D reconstruction of large scenes. S2D clearly outperforms the above methods, and also shows much improvement comparing with sparse-view reconstruction solution DIFIX.

Qualitative results. The qualitative results are shown in Figure 4 for more visual comparison. For 180° view range with six input images, generative method SEVA [79] provides inconsistent details (e.g. the statue and extra pole to the left), and feed-forward methods [17, 62] either suffer from limited view range or flying artifacts. While traditional methods [19, 25] inevitably face large artifacts, the scene reconstructed using DIFIX [58] enhancement still can’t avoid them, which degrades more in 360° view range. Only our method provides the most stable and clean reconstruction under inputs with different sparsity.

Meanwhile, we also showcase the artifact removal ability under another demanding input settings. With only one input, the 3DGS result not only shows severe artifacts, but also suffers from position jitter. Operating on the same 3DGS artifact image, the result of DIFIX is quite blurry and the position can not be fixed, while our result is correct and neat. All the above results show that our pipeline is the strongest in terms of sparse inputs.

4.4. Comparison on driving scenes

In driving scenes, although the input sequence is long, both the large capture distance and the nature of single trajectory could cause significant artifacts in reconstructed scenes, where a solution is also being expected. In this case, we also evaluate our method’s ability when applied to driving scene reconstruction.

| Methods | Interpolation | | Lane Shift @ FID \downarrow | | |
|---------------------|-----------------|--------------------|-------------------------------|-------------|-------------|
| | PSNR \uparrow | LPIPS \downarrow | side 2m | side 3m | up 1.5m |
| EmerNeRF[67] | 25.32 | 0.20 | 96.4 | 101.3 | 90.2 |
| StreetGaussians[64] | 30.14 | 0.14 | 75.0 | 96.7 | 70.3 |
| StreetCrafter[65] | 29.31 | 0.10 | 57.4 | 66.4 | 59.0 |
| DIFIX[58] | 30.26 | 0.11 | 60.2 | 71.6 | 60.3 |
| S2D (Ours) | 31.44 | 0.07 | 46.1 | 53.9 | 41.3 |

Table 2. Quantitative results on Waymo Open Dataset.

Quantitative results. For view interpolation on input trajectory, we compare with base driving scene reconstruction methods StreetGaussians [64] and EmerNeRF [67]. For view extrapolation with lane shifts, we mainly compare with StreetCrafter [65] and DIFIX [58]. The shift setting is similar to StreetCrafter with side shift (left and right) and up shift.

The results are provided in Table 2, where base reconstruction methods shows extremely high FID in shifted views due to large artifacts. While DIFIX can fix small artifacts to improve quality on interpolated views, its lane shift FID is higher than StreetCrafter which uses a video generation model trained on driving scenes for novel trajectory generation. In contrast, our method shows good capability in driving scene reconstruction and outperforms previous methods on both view interpolation and extrapolation.

Qualitative results. We also provide qualitative results in Figure 4 Bottom and Appendix. In Figure 4 is comparison of interpolated front camera views from NuScenes [4] dataset. The direct video generation from SEVA [79] creates inconsistent background objects. Operating on the artifact rendering from StreetGS, the image fixed by DIFIX has clear deformation on lane lines, and the road is also less smooth comparing with our method. More comparison can be found in Appendix.

5. Ablation Studies

We demonstrate the rationality of our design by conduct ablation studies.



Figure 5. Comparison of artifact removal with ablations on guidance mixing.

Table 3. Ablation on dual guidance in artifact fixer.

| # | Ablations | PSNR \uparrow | LPIPS \downarrow |
|---|-----------------------------|-----------------|--------------------|
| ① | Generation from point cloud | 12.7 | 0.71 |
| ② | Mixing latents | 15.6 | 0.49 |
| ③ | No mixing | 19.0 | 0.38 |
| ④ | Dual guidance w/o DINO | 22.1 | 0.27 |
| ⑤ | Dual guidance w DINO | 23.0 | 0.26 |

5.1. Guidance Mixing

We first conduct ablations on the artifact fixer by analyzing current dual guidance design. The first comparison is to use only point cloud rendering and reference view for fixed view generation. The idea is to utilize both structure information from point cloud and background information from reference view, but the model fails to recover accurate background in a single denoising step (①).

When removing the mixing module for the input view, we directly batch point cloud rendering and reference view together with artifact image through multi-view UNet as in DIFIX [58], where we found the model tends to overlook the point cloud input and uses only other images (③), while using DINO guidance will help with balanced attention during the mixing, which is useful to some extent but not significant (④ & ⑤). We believe this is because the early loss is mainly dominated by general image quality, thus the detailed structural guidance of point cloud is covered up.

We also test putting mixing module after VAE block which directly operates upon encoded latents, and we found the results to be overly smoothed (②). Such operation on latents may have caused the targets to drift away from the original space determined by denoising backbone.

The statistical and qualitative ablation results are shown in Table 3 and Figure 5, which prove the rationality of current artifact fixer design.

5.2. Reconstruction Strategy

We also conduct ablations on our reconstruction strategy, which is important in consistent 3D lifting.

Small inconsistency is inevitable with large view range, especially in areas unseen from limited input views. In this case, random sample drop first ensure stable presence of



Figure 6. Ablations on reconstruction strategy. WG indicates weighted gradient, and RSD for random sample drop.

input views, and weighted gradient further constrain the update of wrong areas.

The iterative training stack maintained by random sample drop can provide sufficient 3D correct guidance from input views. Without this behavior, structural details such as textures or small texts (which is a common difficulty for generative methods) will be averaged by novel guidance, as shown in Figure 6 (line 1 middle).

For larger inconsistency occurred in severe artifacts, weighted gradient plays a bigger role. As shown in Figure 6, the large artifacts can not be simply resolved by more samples from input views, and weighted gradient is important in stopping the permanent update of corrupted areas that are also missing in point cloud guidance.

In general, the above ablations prove the necessity of our design for artifact fixer and reconstruction strategy.

For more discussion and demonstration, please refer to Supplementary Material.

6. Conclusion

In this paper, we present Sparse to Dense lifting (S2D), a flexible novel pipeline that enables 3DGS reconstruction with minimal inputs. We present a strong and efficient diffusion fixer for high fidelity artifact fixing along with corresponding reconstruction strategy for robust model fitting.

Experiments shows that our method provides the first-tier results, while the rationality of core components are proven with comprehensive ablation studies. S2D can be easily applied to most 3DGS methods to largely reduce their input requirements, encouraging more general 3DGS applications in real-world situations.

Acknowledgements

This work was supported by the National Natural Science Foundation of China (Grant Nos. 72192821, 62302297, 62302167, 62472282, 62222602, 62502159, U23A20343, W2521174), the Shanghai Committee of Science and Technology (Grant Nos. 25511103300, 25511104302, 25511102700), the Fundamental Research Funds for the Central Universities (project number: YG2023QNA35), YuCaiKe [2023] Project Number: 231111310300, and the Young Elite Scientists Sponsorship Program by CAST YESS20240780.

References

- [1] Jonathan T. Barron, Ben Mildenhall, Dor Verbin, Pratul P. Srinivasan, and Peter Hedman. Mip-nerf 360: Unbounded anti-aliased neural radiance fields. *CVPR*, 2022. 6
- [2] Andreas Blattmann, Tim Dockhorn, Sumith Kulal, Daniel Mendelevitch, Maciej Kilian, Dominik Lorenz, Yam Levi, Zion English, Vikram Voleti, Adam Letts, et al. Stable video diffusion: Scaling latent video diffusion models to large datasets. *arXiv preprint arXiv:2311.15127*, 2023. 3
- [3] Johann Cabon, Lucas Stofl, Leonid Antsfeld, Gabriela Csurka, Boris Chidlovskii, Jerome Revaud, and Vincent Leroy. Must3r: Multi-view network for stereo 3d reconstruction. In *Proceedings of the Computer Vision and Pattern Recognition Conference*, pages 1050–1060, 2025. 2
- [4] Holger Caesar, Varun Bankiti, Alex H Lang, Sourabh Vora, Venice Erin Liong, Qiang Xu, Anush Krishnan, Yu Pan, Giancarlo Baldan, and Oscar Beijbom. nuscenes: A multi-modal dataset for autonomous driving. In *Proceedings of the IEEE/CVF conference on computer vision and pattern recognition*, pages 11621–11631, 2020. 7
- [5] Yuanhao Cai, He Zhang, Kai Zhang, Yixun Liang, Mengwei Ren, Fujun Luan, Qing Liu, Soo Ye Kim, Jianming Zhang, Zhifei Zhang, Yuqian Zhou, Yulun Zhang, Xiaokang Yang, Zhe Lin, and Alan Yuille. Baking gaussian splatting into diffusion denoiser for fast and scalable single-stage image-to-3d generation and reconstruction. In *ICCV*, 2025. 3, 2
- [6] David Charatan, Sizhe Lester Li, Andrea Tagliasacchi, and Vincent Sitzmann. pixelsplat: 3d gaussian splats from image pairs for scalable generalizable 3d reconstruction. In *Proceedings of the IEEE/CVF conference on computer vision and pattern recognition*, pages 19457–19467, 2024. 2
- [7] Yuedong Chen, Haofei Xu, Chuanxia Zheng, Bohan Zhuang, Marc Pollefeys, Andreas Geiger, Tat-Jen Cham, and Jianfei Cai. Mvsplat: Efficient 3d gaussian splatting from sparse multi-view images. In *European Conference on Computer Vision (ECCV)*, 2024. 2
- [8] Yihang Chen, Qianyi Wu, Mengyao Li, Weiyao Lin, Mehrtash Harandi, and Jianfei Cai. Fast feedforward 3d gaussian splatting compression. In *The Thirteenth International Conference on Learning Representations*, 2025. 6, 2
- [9] Kai Deng, Zexin Ti, Jiawei Xu, Jian Yang, and Jin Xie. Vggt-long: Chunk it, loop it, align it – pushing vggt’s limits on kilometer-scale long rgb sequences, 2025. 3
- [10] Siyan Dong, Shuzhe Wang, Shaohui Liu, Lulu Cai, Qingnan Fan, Juho Kannala, and Yanchao Yang. Reloc3r: Large-scale training of relative camera pose regression for generalizable, fast, and accurate visual localization. *arXiv preprint arXiv:2412.08376*, 2024. 3
- [11] Bardenius Pieter Duisterhof, Lojze Zust, Philippe Weinzaepfel, Vincent Leroy, Johann Cabon, and Jerome Revaud. Mast3r-sfm: a fully-integrated solution for unconstrained structure-from-motion. In *2025 International Conference on 3D Vision (3DV)*, pages 1–10. IEEE, 2025. 2
- [12] Sven Elflein, Qunjie Zhou, and Laura Leal-Taixé. Light3r-sfm: Towards feed-forward structure-from-motion. In *Proceedings of the Computer Vision and Pattern Recognition Conference*, pages 16774–16784, 2025. 2
- [13] Lue Fan, Hao Zhang, Qitai Wang, Hongsheng Li, and Zhaoxiang Zhang. Freesim: Toward free-viewpoint camera simulation in driving scenes. In *Proceedings of the Computer Vision and Pattern Recognition Conference*, pages 12004–12014, 2025. 3
- [14] Ruiqi Gao*, Aleksander Holynski*, Philipp Henzler, Arthur Brussee, Ricardo Martin-Brualla, Pratul P. Srinivasan, Jonathan T. Barron, and Ben Poole*. Cat3d: Create anything in 3d with multi-view diffusion models. *Advances in Neural Information Processing Systems*, 2024. 3
- [15] Martin Heusel, Hubert Ramsauer, Thomas Unterthiner, Bernhard Nessler, and Sepp Hochreiter. Gans trained by a two time-scale update rule converge to a local nash equilibrium. *Advances in neural information processing systems*, 30, 2017. 6
- [16] Edward J Hu, Yelong Shen, Phillip Wallis, Zeyuan Allen-Zhu, Yuanzhi Li, Shean Wang, Lu Wang, Weizhu Chen, et al. Lora: Low-rank adaptation of large language models. *ICLR*, 1(2):3, 2022. 4
- [17] Lihan Jiang, Yucheng Mao, Linning Xu, Tao Lu, Kerui Ren, Yichen Jin, Xudong Xu, Mulin Yu, Jiangmiao Pang, Feng Zhao, et al. Anysplat: Feed-forward 3d gaussian splatting from unconstrained views. *arXiv preprint arXiv:2505.23716*, 2025. 2, 7
- [18] Nikhil Keetha, Norman Müller, Johannes Schönberger, Lorenzo Porzi, Yuchen Zhang, Tobias Fischer, Arno Knapitsch, Duncan Zauss, Ethan Weber, Nelson Antunes, Jonathon Luiten, Manuel Lopez-Antequera, Samuel Rota Bulò, Christian Richardt, Deva Ramanan, Sebastian Scherer, and Peter Kotschieder. MapAnything: Universal feed-forward metric 3D reconstruction, 2025. arXiv preprint arXiv:2509.13414. 2, 3
- [19] Bernhard Kerbl, Georgios Kopanas, Thomas Leimkühler, and George Drettakis. 3d gaussian splatting for real-time radiance field rendering. *ACM Trans. Graph.*, 42(4):139–1, 2023. 1, 2, 6, 7
- [20] Vincent Leroy, Johann Cabon, and Jérôme Revaud. Grounding image matching in 3d with mast3r. In *European Conference on Computer Vision*, pages 71–91. Springer, 2024. 2
- [21] Lu Ling, Yichen Sheng, Zhi Tu, Wentian Zhao, Cheng Xin, Kun Wan, Lantao Yu, Qianyu Guo, Zixun Yu, Yawen Lu, et al. D13dv-10k: A large-scale scene dataset for deep learning-based 3d vision. In *Proceedings of the IEEE/CVF*

- Conference on Computer Vision and Pattern Recognition*, pages 22160–22169, 2024. 6, 2
- [22] Kunhao Liu, Fangneng Zhan, Jiahui Zhang, Muyu Xu, Yingchen Yu, Abdulmoteleb El Saddik, Christian Theobalt, Eric Xing, and Shijian Lu. Weakly supervised 3d open-vocabulary segmentation. *arXiv preprint arXiv:2305.14093*, 2023. 6
- [23] Ruoshi Liu, Rundi Wu, Basile Van Hoorick, Pavel Tokmakov, Sergey Zakharov, and Carl Vondrick. Zero-1-to-3: Zero-shot one image to 3d object, 2023. 3
- [24] Yang Liu, Chuanchen Luo, Lue Fan, Naiyan Wang, Junran Peng, and Zhaoxiang Zhang. Citygaussian: Real-time high-quality large-scale scene rendering with gaussians. In *European Conference on Computer Vision*, pages 265–282. Springer, 2025. 2
- [25] Tao Lu, Mulin Yu, Linning Xu, Yuanbo Xiangli, Limin Wang, Dahua Lin, and Bo Dai. Scaffold-gs: Structured 3d gaussians for view-adaptive rendering. In *Proceedings of the IEEE/CVF Conference on Computer Vision and Pattern Recognition*, pages 20654–20664, 2024. 7
- [26] Yiren Lu, Yunlai Zhou, Disheng Liu, Tuo Liang, and Yu Yin. Bard-gs: Blur-aware reconstruction of dynamic scenes via gaussian splatting. In *Proceedings of the Computer Vision and Pattern Recognition Conference*, pages 16532–16542, 2025. 2
- [27] Riku Murai, Eric Dexheimer, and Andrew J Davison. Mast3r-slam: Real-time dense slam with 3d reconstruction priors. In *Proceedings of the Computer Vision and Pattern Recognition Conference*, pages 16695–16705, 2025. 2
- [28] Chaojun Ni, Guosheng Zhao, Xiaofeng Wang, Zheng Zhu, Wenkang Qin, Guan Huang, Chen Liu, Yuyin Chen, Yida Wang, Xueyang Zhang, et al. Recondreamer: Crafting world models for driving scene reconstruction via online restoration. In *Proceedings of the Computer Vision and Pattern Recognition Conference*, pages 1559–1569, 2025. 3, 5
- [29] Gaurav Parmar, Taesung Park, Srinivasa Narasimhan, and Jun-Yan Zhu. One-step image translation with text-to-image models. *arXiv preprint arXiv:2403.12036*, 2024. 3, 4, 1
- [30] Zador Pataki, Paul-Edouard Sarlin, Johannes L Schönberger, and Marc Pollefeys. Mp-sfm: Monocular surface priors for robust structure-from-motion. In *Proceedings of the Computer Vision and Pattern Recognition Conference*, pages 21891–21901, 2025. 2
- [31] Zhexi Peng, Kun Zhou, and Tianjia Shao. Gaussian-plus-sdf slam: High-fidelity 3d reconstruction at 150+ fps. *Computational Visual Media*, 2025. 2
- [32] Dustin Podell, Zion English, Kyle Lacey, Andreas Blattmann, Tim Dockhorn, Jonas Müller, Joe Penna, and Robin Rombach. Sdxl: Improving latent diffusion models for high-resolution image synthesis. *arXiv preprint arXiv:2307.01952*, 2023. 3
- [33] Alec Radford, Jong Wook Kim, Chris Hallacy, Aditya Ramesh, Gabriel Goh, Sandhini Agarwal, Girish Sastry, Amanda Askell, Pamela Mishkin, Jack Clark, et al. Learning transferable visual models from natural language supervision. In *International conference on machine learning*, pages 8748–8763. PmLR, 2021. 4
- [34] Robin Rombach, Andreas Blattmann, Dominik Lorenz, Patrick Esser, and Björn Ommer. High-resolution image synthesis with latent diffusion models. In *Proceedings of the IEEE/CVF conference on computer vision and pattern recognition*, pages 10684–10695, 2022. 3
- [35] Olaf Ronneberger, Philipp Fischer, and Thomas Brox. U-net: Convolutional networks for biomedical image segmentation. In *Medical image computing and computer-assisted intervention—MICCAI 2015: 18th international conference, Munich, Germany, October 5–9, 2015, proceedings, part III 18*, pages 234–241. Springer, 2015. 3
- [36] Kyle Sargent, Zizhang Li, Tanmay Shah, Charles Herrmann, Hong-Xing Yu, Yunzhi Zhang, Eric Ryan Chan, Dmitry Lagun, Li Fei-Fei, Deqing Sun, and Jiajun Wu. ZeroNVS: Zero-shot 360-degree view synthesis from a single real image. *arXiv preprint arXiv:2310.17994*, 2023. 3
- [37] Axel Sauer, Dominik Lorenz, Andreas Blattmann, and Robin Rombach. Adversarial diffusion distillation, 2023. 4
- [38] Pei Sun, Henrik Kretzschmar, Xerxes Dotiwalla, Aurelien Chouard, Vijaysai Patnaik, Paul Tsui, James Guo, Yin Zhou, Yuning Chai, Benjamin Caine, et al. Scalability in perception for autonomous driving: Waymo open dataset. In *Proceedings of the IEEE/CVF conference on computer vision and pattern recognition*, pages 2446–2454, 2020. 6, 2
- [39] Su Sun, Cheng Zhao, Zhuoyang Sun, Yingjie Victor Chen, and Mei Chen. Splatflow: Self-supervised dynamic gaussian splatting in neural motion flow field for autonomous driving. In *Proceedings of the Computer Vision and Pattern Recognition Conference*, pages 27487–27496, 2025. 2
- [40] Stanislaw Szymonowicz, Christian Rupprecht, and Andrea Vedaldi. Splatter image: Ultra-fast single-view 3d reconstruction. In *Proceedings of the IEEE/CVF conference on computer vision and pattern recognition*, pages 10208–10217, 2024. 2
- [41] Jiaxiang Tang, Jiawei Ren, Hang Zhou, Ziwei Liu, and Gang Zeng. Dreamgaussian: Generative gaussian splatting for efficient 3d content creation. *arXiv preprint arXiv:2309.16653*, 2023. 2
- [42] Jiaxiang Tang, Zhaoxi Chen, Xiaokang Chen, Tengfei Wang, Gang Zeng, and Ziwei Liu. Lgm: Large multi-view gaussian model for high-resolution 3d content creation. In *European Conference on Computer Vision*, pages 1–18. Springer, 2024. 2
- [43] Zhenggang Tang, Yuchen Fan, Dilin Wang, Hongyu Xu, Rakesh Ranjan, Alexander Schwing, and Zhicheng Yan. Mv-dust3r+: Single-stage scene reconstruction from sparse views in 2 seconds. *arXiv preprint arXiv:2412.06974*, 2024. 3
- [44] Qijian Tian, Xin Tan, Yuan Xie, and Lizhuang Ma. Drivingforward: Feed-forward 3d gaussian splatting for driving scene reconstruction from flexible surround-view input. In *Proceedings of the AAAI Conference on Artificial Intelligence*, 2025. 2
- [45] Vikram Voleti, Chun-Han Yao, Mark Boss, Adam Letts, David Pankratz, Dmitrii Tochilkin, Christian Laforte, Robin Rombach, and Varun Jampani. SV3D: Novel multi-view synthesis and 3D generation from a single image using la-

- tent video diffusion. In *European Conference on Computer Vision (ECCV)*, 2024. 2, 3
- [46] Chen Wang, Hao-Yang Peng, Ying-Tian Liu, Jiatao Gu, and Shi-Min Hu. Diffusion models for 3d generation: A survey. *Computational Visual Media*, 11(1):1–28, 2025. 3
- [47] Hengyi Wang and Lourdes Agapito. 3d reconstruction with spatial memory. *arXiv preprint arXiv:2408.16061*, 2024. 2
- [48] Jianyuan Wang, Minghao Chen, Nikita Karaev, Andrea Vedaldi, Christian Rupprecht, and David Novotny. Vggt: Visual geometry grounded transformer. In *Proceedings of the IEEE/CVF Conference on Computer Vision and Pattern Recognition*, 2025. 2, 3
- [49] Qianqian Wang, Yifei Zhang, Aleksander Holynski, Alexei A Efros, and Angjoo Kanazawa. Continuous 3d perception model with persistent state. In *Proceedings of the Computer Vision and Pattern Recognition Conference*, pages 10510–10522, 2025. 2
- [50] Shuzhe Wang, Vincent Leroy, Yohann Cabon, Boris Chidlovskii, and Jerome Revaud. Dust3r: Geometric 3d vision made easy. In *Proceedings of the IEEE/CVF Conference on Computer Vision and Pattern Recognition*, pages 20697–20709, 2024. 2
- [51] Weijie Wang, Yeqing Chen, Zeyu Zhang, Hengyu Liu, Haoxiao Wang, Zhiyuan Feng, Wenkang Qin, Zheng Zhu, Donny Y Chen, and Bohan Zhuang. Volsplat: Rethinking feed-forward 3d gaussian splatting with voxel-aligned prediction. *arXiv preprint arXiv:2509.19297*, 2025. 2
- [52] Xiaofeng Wang, Kang Zhao, Feng Liu, Jiayu Wang, Guosheng Zhao, Xiaoyi Bao, Zheng Zhu, Yingya Zhang, and Xingang Wang. Egovid-5m: A large-scale video-action dataset for egocentric video generation. *arXiv preprint arXiv:2411.08380*, 2024. 3
- [53] Xiaofeng Wang, Zheng Zhu, Guan Huang, Xinze Chen, Jiayang Zhu, and Jiwen Lu. Drivedreamer: Towards real-world-drive world models for autonomous driving. In *European Conference on Computer Vision*, pages 55–72. Springer, 2024. 3
- [54] Yifan Wang, Jianjun Zhou, Haoyi Zhu, Wenzheng Chang, Yang Zhou, Zizun Li, Junyi Chen, Jiangmiao Pang, Chunhua Shen, and Tong He. π^3 : Scalable permutation-equivariant visual geometry learning, 2025. 2, 3
- [55] Zhouxia Wang, Ziyang Yuan, Xintao Wang, Yaowei Li, Tianshui Chen, Menghan Xia, Ping Luo, and Ying Shan. Motionctrl: A unified and flexible motion controller for video generation. In *ACM SIGGRAPH 2024 Conference Papers*, pages 1–11, 2024. 2, 3
- [56] Daniel Watson, Saurabh Saxena, Lala Li, Andrea Tagliasacchi, and David J. Fleet. Controlling space and time with diffusion models, 2025. 2
- [57] Jiaxin Wei, Stefan Leutenegger, and Simon Schaefer. Gsfix3d: Diffusion-guided repair of novel views in gaussian splatting, 2025. 3
- [58] Jay Zhangjie Wu, Yuxuan Zhang, Haithem Turki, Xuanchi Ren, Jun Gao, Mike Zheng Shou, Sanja Fidler, Zan Gojic, and Huan Ling. Difix3d+: Improving 3d reconstructions with single-step diffusion models. In *Proceedings of the Computer Vision and Pattern Recognition Conference*, pages 26024–26035, 2025. 2, 3, 4, 5, 7, 8
- [59] Rundi Wu, Ben Mildenhall, Philipp Henzler, Keunhong Park, Ruiqi Gao, Daniel Watson, Pratul P. Srinivasan, Dor Verbin, Jonathan T. Barron, Ben Poole, and Aleksander Holynski. Reconfusion: 3d reconstruction with diffusion priors. *arXiv*, 2023. 3
- [60] Tong Wu, Yu-Jie Yuan, Ling-Xiao Zhang, Jie Yang, Yan-Pei Cao, Ling-Qi Yan, and Lin Gao. Recent advances in 3d gaussian splatting. *Computational Visual Media*, 10(4):613–642, 2024. 2
- [61] Tao Xie, Xi Chen, Zhen Xu, Yiman Xie, Yudong Jin, Yujun Shen, Sida Peng, Hujun Bao, and Xiaowei Zhou. Envgs: Modeling view-dependent appearance with environment gaussian. In *Proceedings of the Computer Vision and Pattern Recognition Conference*, pages 5742–5751, 2025. 2
- [62] Haofei Xu, Songyou Peng, Fangjinhua Wang, Hermann Blum, Daniel Barath, Andreas Geiger, and Marc Pollefeys. Depthsplat: Connecting gaussian splatting and depth. In *Proceedings of the Computer Vision and Pattern Recognition Conference*, pages 16453–16463, 2025. 2, 7
- [63] Yinghao Xu, Zifan Shi, Wang Yifan, Hansheng Chen, Ceyuan Yang, Sida Peng, Yujun Shen, and Gordon Wetstein. Grm: Large gaussian reconstruction model for efficient 3d reconstruction and generation. In *European Conference on Computer Vision*, pages 1–20. Springer, 2024. 2
- [64] Yunzhi Yan, Haotong Lin, Chenxu Zhou, Weijie Wang, Haiyang Sun, Kun Zhan, Xianpeng Lang, Xiaowei Zhou, and Sida Peng. Street gaussians: Modeling dynamic urban scenes with gaussian splatting. In *European Conference on Computer Vision*, pages 156–173. Springer, 2024. 7
- [65] Yunzhi Yan, Zhen Xu, Haotong Lin, Haiyan Jin, Haoyu Guo, Yida Wang, Kun Zhan, Xianpeng Lang, Hujun Bao, Xiaowei Zhou, et al. Streetcrafter: Street view synthesis with controllable video diffusion models. In *Proceedings of the Computer Vision and Pattern Recognition Conference*, pages 822–832, 2025. 3, 5, 7, 2
- [66] Chen Yang, Sikuang Li, Jiemin Fang, Ruofan Liang, Lingxi Xie, Xiaopeng Zhang, Wei Shen, and Qi Tian. Gaussianobject: High-quality 3d object reconstruction from four views with gaussian splatting. *ACM Transactions on Graphics*, 2024. 2
- [67] Jiawei Yang, Boris Ivanovic, Or Litany, Xinshuo Weng, Seung Wook Kim, Boyi Li, Tong Che, Danfei Xu, Sanja Fidler, Marco Pavone, et al. Emernerf: Emergent spatial-temporal scene decomposition via self-supervision. *arXiv preprint arXiv:2311.02077*, 2023. 7
- [68] Jianing Yang, Alexander Sax, Kevin J. Liang, Mikael Henaff, Hao Tang, Ang Cao, Joyce Chai, Franziska Meier, and Matt Feiszli. Fast3r: Towards 3d reconstruction of 1000+ images in one forward pass. In *Proceedings of the IEEE/CVF Conference on Computer Vision and Pattern Recognition (CVPR)*, 2025. 3
- [69] Zhuoyi Yang, Jiayan Teng, Wendi Zheng, Ming Ding, Shiyu Huang, Jiazheng Xu, Yuanming Yang, Wenyi Hong, Xiaohan Zhang, Guanyu Feng, et al. Cogvideox: Text-to-video diffusion models with an expert transformer. *arXiv preprint arXiv:2408.06072*, 2024. 3
- [70] Botao Ye, Sifei Liu, Haofei Xu, Li Xueting, Marc Pollefeys, Ming-Hsuan Yang, and Peng Songyou. No pose, no problem:

- Surprisingly simple 3d gaussian splats from sparse unposed images. *arXiv preprint arXiv:2410.24207*, 2024. [2](#), [7](#)
- [71] Wangbo Yu, Jinbo Xing, Li Yuan, Wenbo Hu, Xiaoyu Li, Zhipeng Huang, Xiangjun Gao, Tien-Tsin Wong, Ying Shan, and Yonghong Tian. Viewcrafter: Taming video diffusion models for high-fidelity novel view synthesis. *arXiv preprint arXiv:2409.02048*, 2024. [2](#), [3](#), [7](#)
- [72] Zehao Yu, Torsten Sattler, and Andreas Geiger. Gaussian opacity fields: Efficient adaptive surface reconstruction in unbounded scenes. *ACM Transactions on Graphics*, 2024. [7](#)
- [73] Kai Zhang, Sai Bi, Hao Tan, Yuanbo Xiangli, Nanxuan Zhao, Kalyan Sunkavalli, and Zexiang Xu. Gs-lrm: Large reconstruction model for 3d gaussian splatting. In *European Conference on Computer Vision*, pages 1–19. Springer, 2024. [2](#)
- [74] Richard Zhang, Phillip Isola, Alexei A Efros, Eli Shechtman, and Oliver Wang. The unreasonable effectiveness of deep features as a perceptual metric. In *Proceedings of the IEEE conference on computer vision and pattern recognition*, pages 586–595, 2018. [6](#)
- [75] Guosheng Zhao, Chaojun Ni, Xiaofeng Wang, Zheng Zhu, Xueyang Zhang, Yida Wang, Guan Huang, Xinze Chen, Boyuan Wang, Youyi Zhang, et al. Drivedreamer4d: World models are effective data machines for 4d driving scene representation. In *Proceedings of the Computer Vision and Pattern Recognition Conference*, pages 12015–12026, 2025. [3](#), [5](#)
- [76] Guosheng Zhao, Xiaofeng Wang, Chaojun Ni, Zheng Zhu, Wenkang Qin, Guan Huang, and Xingang Wang. Recondreamer++: Harmonizing generative and reconstructive models for driving scene representation. *arXiv preprint arXiv:2503.18438*, 2025. [3](#), [5](#)
- [77] Guosheng Zhao, Xiaofeng Wang, Zheng Zhu, Xinze Chen, Guan Huang, Xiaoyi Bao, and Xingang Wang. Drivedreamer-2: Llm-enhanced world models for diverse driving video generation. In *Proceedings of the AAAI Conference on Artificial Intelligence*, pages 10412–10420, 2025. [3](#)
- [78] Jianhao Zheng, Zihan Zhu, Valentin Bieri, Marc Pollefeys, Songyou Peng, and Armeni Iro. Wildgs-slam: Monocular gaussian splatting slam in dynamic environments. In *Proceedings of the IEEE/CVF Conference on Computer Vision and Pattern Recognition (CVPR)*, 2025. [2](#)
- [79] Jensen (Jinghao) Zhou, Hang Gao, Vikram Voleti, Aaryaman Vasishtha, Chun-Han Yao, Mark Boss, Philip Torr, Christian Rupprecht, and Varun Jampani. Stable virtual camera: Generative view synthesis with diffusion models. *arXiv preprint arXiv:2503.14489*, 2025. [2](#), [3](#), [7](#)
- [80] Tinghui Zhou, Richard Tucker, John Flynn, Graham Fyffe, and Noah Snavely. Stereo magnification: Learning view synthesis using multiplane images, 2018. [6](#)
- [81] Zi-Xin Zou, Zhipeng Yu, Yuan-Chen Guo, Yangguang Li, Ding Liang, Yan-Pei Cao, and Song-Hai Zhang. Triplane meets gaussian splatting: Fast and generalizable single-view 3d reconstruction with transformers. *arXiv preprint arXiv:2312.09147*, 2023. [2](#)

S2D: Sparse to Dense Lifting for 3D Reconstruction with Minimal Inputs

Supplementary Material

| Ablations | PSNR \uparrow | LPIPS \downarrow |
|---|-----------------|--------------------|
| $\mathcal{L}_{LPIPS} + \mathcal{L}_2 + \mathcal{L}_{GAN} + \mathcal{L}_{CLIP}$ | 20.1 | 0.35 |
| $\mathcal{L}_{LPIPS} + \mathcal{L}_2 + \mathcal{L}_{GAN}$ | 20.1 | 0.35 |
| $\mathcal{L}_{LPIPS} + \mathcal{L}_2 + \mathcal{L}_{GAN} + \mathcal{L}_{DINO}$ | 20.5 | 0.33 |
| $\mathcal{L}_{LPIPS} + \mathcal{L}_2 + \mathcal{L}_{GAN} + \mathcal{L}_{SSIM}$ | 21.8 | 0.28 |
| $\mathcal{L}_{LPIPS} + \mathcal{L}_2 + \mathcal{L}_{GAN} + \mathcal{L}_{SSIM} + \mathcal{L}_{DINO}$ | 22.0 | 0.27 |

Table 4. Ablation on loss terms.



Figure 7. Training data with different levels of artifacts (line 1) and example of random perturbations (line 2).

7. Ablation on loss terms

We further conduct ablations on loss terms applied on S2D artifact fixer by evaluating the image quality conditioned on different loss choices. Apart from base losses that are already verified [29], we compare the difference of CLIP, DINO and SSIM losses. The results are reported in Table 4.

While this is not new image generation task, the original CLIP loss actually contributes nothing in training, thus removing CLIP loss makes completely no difference. Introducing SSIM loss provides more improvements with higher supervision on structural details. DINO loss also helps with small enhancement by aligning semantic features.

We also test applying different weights to each loss term, and the results remain unchanged across reasonable variation within the range of 0.4.

8. Training data

To enhance the robustness of our model, we generate an extensive dataset that covers the broadest spectrum of corruption boundaries.

The processed training data with different artifact levels is shown in Figure 7 Line 1. To demonstrate how random perturbations introduced in Sec 3.3 works, we also provide an example of render-time perturbation on correctly reconstructed 3DGS scenes in Figure 7 Line 2, where the perturbation intensity increases from left to right.

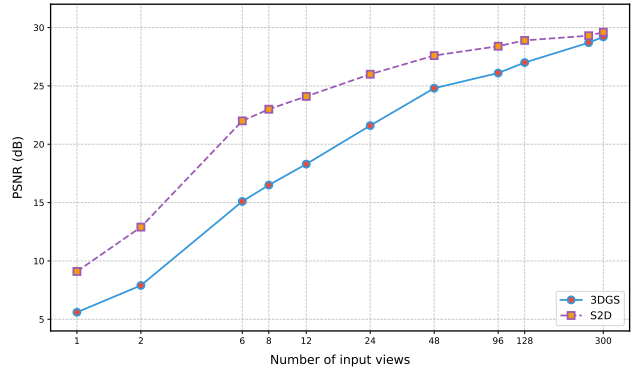


Figure 8. Reconstruction quality versus input density.

The large artifacts guide the model to recover basic object structure, while the perturbation applied on mild corruptions can further encourage detail enhancements, especially textures and edges. Therefore, our model is able to handle a large range of input intensity.

9. Evaluation on input density

We evaluate S2D’s ability when faced with different amount of input images, the results on DL3DV scenes are provided in Figure 8.

As shown, our reconstruction quality improves steadily when increasing the number of input views. S2D consistently outperforms 3DGS with large improvements in sparse input and extra enhancement in dense input settings. This shows that S2D can be applied in general situations instead of fixed input views.

10. Performance report

The computational cost of S2D fixer is low, including 11.1 GB GPU usage and 1 FPS processing speed upon image resolution 1024×576 on a single RTX 4090. Under the same setting, Stable Virtual Camera (SEVA) results in 16.4 GB GPU usage and 0.08 FPS generation speed, while DIFIX is on par with S2D with 10.9 GPU usage and 1 FPS processing speed.

The reported processing speed means that the generation of novel guidance with S2D creates very small overhead comparing with original reconstruction (*e.g.* on 3DOVS dataset, with 30 seconds fixing is only 1/30 of the total 15 minutes reconstruction), empowering the application of S2D in diverse scheme combinations while eliminating concerns about noticeable efficiency degradation.



Figure 9. Extra results of DiffusionGS and driving scene comparison.

11. More Comparison

We provide more qualitative comparison in Figure 9. For the same scenes as in Figure 4, the latest sparse-view reconstruction method DiffusionGS [5] (mainly object-centric) largely degrades with respect to in-the-wild scenes.

In line 2 we compare the side camera results on Waymo Open Dataset [38]. Operating on the same artifact image, DIFIX generates wrong car details and fuzzy road with supersaturated lane lines, while ours is more consistent.

12. More Implementation Details

Due to the page limit of the main paper, we provide more implementation details and discussion here.

Evaluation standard. While many feed-forward reconstruction researches now tend to conduct evaluation only on a few images from the original scene capture (especially sparse-view reconstruction such as 2-view reconstruction), we believe that this is insufficient to represent the actual and overall reconstruction quality of the complete scene.

Therefore, evaluation results reported in this paper are tested on **all other frames** of a scene that are not used for training or reference, identical to the evaluation standard of traditional reconstruction methods.

Evaluation on static scenes is conducted with the max pixel size of 255000 (the original setting for π^3 [54], e.g. 672×378) per image while remaining the original aspect ratio. This is to align with the default rendered image of point cloud for detail consistency, which is not compulsory. While many feed-forward methods only support fixed resolution or aspect ratio such as 256×256 , S2D can work on any resolution and aspect ratio. In driving scenes, we evaluate the results on resolution 1024×576 as the setting in StreetCrafter [65].

Rendering for point cloud. We render point cloud images generated by VFMs through *pyrender*.

Specifically, we initialize an empty scene with black background, and generate mesh from reconstructed point cloud.

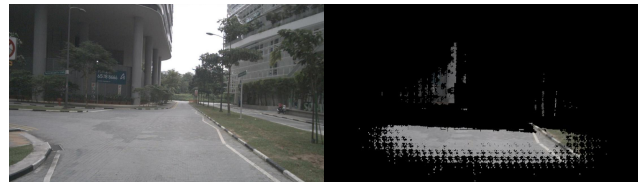


Figure 10. Point cloud rendering with single image input.

We applied *MetallicRoughnessMaterial* with *metallicFactor* set at 1.0 and *baseColorFactor* set as [1.0, 1.0, 1.0, 1.0] to all meshes to maintain the original point color.

Given camera intrinsics and poses, the corresponding point cloud images are then rendered through *Perspective-Camera*.

Data and training. The S2D artifact fixer is trained on our processed DL3DV-960[8, 21] dataset (train split) on 1-7K scenes for 75000 steps. The training images are augmented with random horizontal flip. All images are resized to 512×512 during training. The model is implemented in PyTorch and optimized with the AdamW optimizer, weight dtype is float32.

13. Limitation and future work

While our methods utilize VFM priors, we share the same limitation as VFMs. If the input images are both extremely sparse and low in texture, the resulting point cloud can be quite fragmentary. We show such a failure case in Figure 10 from the NuScenes dataset. This means the point cloud can hardly provide sufficient guidance and the fixing can only work on smaller artifacts. Fortunately, the VFM can be easily replaced to avoid similar situation.

The current fixing model uses point cloud for structural guidance and reference view for textural guidance, but we think the ultimate goal is to directly utilize both structural guidance and textural guidance from reference views while still work as an efficient image-level fixing. We are now working on further spatial feature extraction and cross-attention to pursue this objective.